Master's thesis

NTNU
Norwegian University of Science and Technology

Kristian Bryhn Myhre

The Galactic Magnetic Field: A Comparison of Two Models

Master's thesis in MSPHYS
Supervisor: Michael Kachelriess
December 2019

NTNU
Norwegian University of
Science and Technology

Kristian Bryhn Myhre

The Galactic Magnetic Field: A Comparison of Two Models

Master's thesis in MSPHYS
Supervisor: Michael Kachelriess
December 2019

Norwegian University of Science and Technology

NTNU
Norwegian University of
Science and Technology

Summary

The main observables used to probe the Galactic Magnetic Field, Faraday rotation measure and the total and polarized intensity of synchrotron emission, will be presented along with the Jansson-Farrar model and Sun *et al.* model for the Galactic Magnetic Field. The models will be compared and discussed on the basis of their functional form and how they reproduce the aforementioned observables.

Sammendrag

De viktigste målbare størrelsene for å gjøre målinger på det galaktiske magnetisk feltet, Faradayrotasjonsmål og den totale og polariserte intensiteten til synkrotronstråling, vil bli presentert sammen med Jansson-Farrar-modellen og Sun *et al.*-modellen for det galaktiske magnetiske feltet. Disse modellene vil bli sammenlignet på bakgrunn av deres funksjonelle form og hvordan de reproduserer de ovennevnte målbare størrelsene.

Acknowledgements

Thank you to my supervisor, Michael Kachelriess, for sticking with me through this ordeal,
Thank you to my family, who always support and believe in me,
And thank you to Linjeforeningen Delta, for keeping me sane when too much was spinning through my head.

Contents

Chapter 1

Introduction

Much of our galaxy is made up of plasma, be it the general interstellar medium, stars, jets or specific objects like supernova remnants. Due to this ever present plasma, one would rightly assume there to be a magnetic field permeating the galaxy on a large scale, as Hannes Alfvén was the first to think in 1937 (Alfvén, 1937). This field has garnered much attention and study since its discovery, and the attempts to model it the last couple of decades have become numerous. This thesis will focus on two of the most used models, the Jansson-Farrar model (Jansson and Farrar, 2012) and the Sun *et al.* model (Sun et al., 2008).

The reasons for the interest in this field are many, but the main motivation for modelling it accurately is its influence on the propagation and acceleration of charged particles moving through it from sources both inside and outside the Milky Way. The field also interests the Cosmic Microwave Background community, as it produces polarised synchrotron emission, which acts as a strong foreground for cosmic microwave background polarization.

Fully modelling the Galactic magnetic field is extremely difficult. Our vantage point inside the galaxy does not make the task any easier, because

as a result only two-dimensional tracers are available to probe a three-dimensional field. In addition, it is only possible to detect either the parallel or the perpendicular component at a time, as these are connected to different observables, that in turn are not entirely reliable. This causes the modelling of the Galactic magnetic field to be done with the knowledge that what is modelled might not fully reflect the physical reality.

Normally the Galactic magnetic field is separated into two main parts; the large-scale regular field and the small-scale random field. The large-scale regular field is the field that permeates the entire Galaxy, while the small-scale random field originates from turbulence and self-interaction in the interstellar medium. These parts are often divided into several components as well.

This thesis will first present the main existing ways of probing the Galactic Magnetic Field, and then present the functional forms of the Jansson-Farrar and Sun *et al.* models. Finally these models will be compared to each other and discussed.

Chapter 2

Observables

To be able to have a starting point when building a model for the Galactic Magnetic Field, it is important to have data to base the models on. In addition, one can use a finished model to simulate how the same data will look like when that model is imposed on the galaxy, and use the comparison between the real and simulated data to say something about the viability and accuracy of that model. In this chapter, the three most heavily used observables in the case of the Galactic Magnetic Field – Faraday rotation measures (RM), and the intensity (I) and polarized intensity (I_p) of synchrotron emission – will be examined. In addition, the small-scale random field will be discussed, and the models for the electron densities that will be used while simulating the rotation measures and synchrotron intensities will be described.

2.1 Faraday Rotation Measures

When polarized radiation passes through a magnetic field with a component parallel to the direction of the radiation, a phenomenon called Faraday

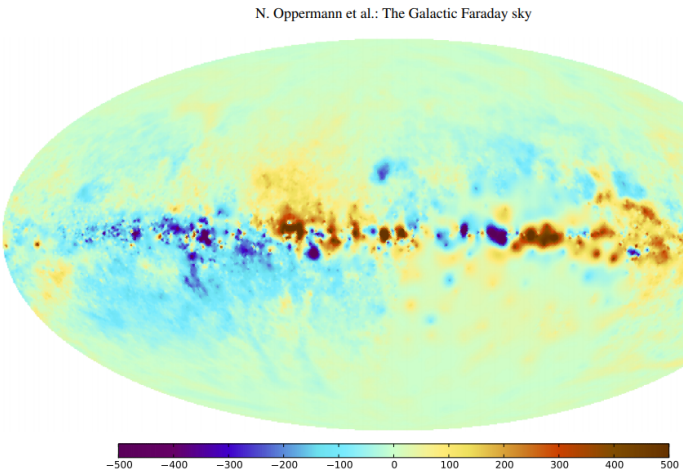

Figure 2.1: Full-sky map of the Faraday rotation measures by Oppermann et al. (2012). The unit of the bar is radians/m^2. Galactic longitude is zero in the centre, increasing to the right.

rotation occurs. This effect is a rotation of the polarization angle θ_0 to θ and is described by

$$\theta = \theta_0 + \mathrm{RM}\lambda, \tag{2.1}$$

where λ is the wavelength of the radiation and RM is the Faraday rotation measure. When the rotation measure data of a Galactic Magnetic Field model is simulated, it is dependent on the thermal electron density n_e and the previously mentioned parallel component of the magnetic field $B_{||}$ as

$$\mathrm{RM} \simeq 0.81 \int_{LOS} \frac{n_e(l)}{\mathrm{cm}^{-3}} \frac{B_{||}(l)}{\mu\mathrm{G}} \frac{\mathrm{d}l}{\mathrm{pc}}, \tag{2.2}$$

where LOS denotes that we integrate along a line of sight to or from Earth through the galaxy. One of the main reasons why this observable is so interesting is that due to the linear dependency on $B_{||}$, the rotation measures say something about both the orientation and direction of the

Galactic Magnetic Field, that is, we can probe both how parallel it is to the line of sight and whether it is pointing towards or away from Earth.

Now that the reason why the rotation measure is interesting to us is clear, it is important to note that there are challenges in obtaining accurate data for it. There are sources of rotation measures in the galaxy that are not the Galactic Magnetic Field. For instance, as is noted in Jansson and Farrar (2012), there is a region fairly close to our solar system that is filled with H1, the most common isotope of hydrogen. This kind of region is called a H1-bubble, and the χ^2 of the data was found to be reduced when the rotation measures from the area of the sky belonging to this bubble were removed entirely from the data set in Jansson and Farrar (2012). More "bubbles" like this can be removed when better rotation measure synthesis is available. It is also possible that the radiation we look at from extragalactic sources is already Faraday rotated when it enters our galaxy, which adds a constant to equation 2.1.

Another case is if the Faraday rotating and synchrotron emitting media are mixed, equation 2.2 instead produces the Faraday depht ϕ with the caveat that the integration boundaries now are dependent on the distance along the line of sight. From ϕ a Faraday spectrum is then derived (Brentjens and de Bruyn, 2005, Burn, 1966). In addition, equation 2.2 assumes that n_e and $B_{||}$ are independent of each other, but if the magnetic field is strong enough to influence the gas distribution, this assumption no longer holds. It has been shown that if the interstellar medium is in pressure equilibrium, n_e and $B_{||}$ are anti-correlated (Beck et al., 2003), which potentially has a big impact on our estimates for the rotation measures. Due to all these uncertainties, an iterative scheme is often used to remove outliers and to smooth local fluctuations in the data. An example of can be found in section 3 of Jansson and Farrar (2012).

A great way to put constraints on the Galactic Magnetic Field is to use rotation measures from pulsars, as the radiation they produce is very well documented. Then we can use a line of sight integral from Earth to the pulsar to examine the magnetic field between the two, and by combining

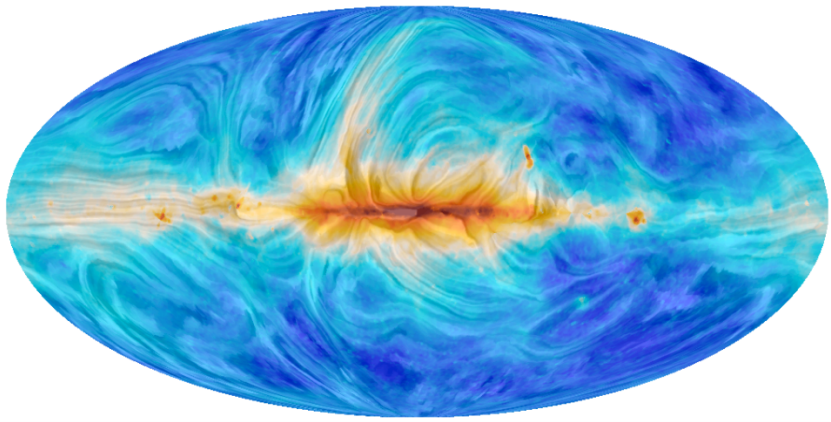

Figure 2.2: Full-sky map of synchrotron emission at 30 GHz from Adam et al. (2016). The colour indicate total intensity and the texture indicate the polarization rotated 90 degrees as to show the orientation of the magnetic field that produced the radiation.

many such integrals obtain a much more three dimensional picture of the Galactic Magnetic Field. Unfortunately, there are not enough pulsars for which we know the exact distance from Earth, and therefore we are unable to use them as reference points due to inaccuracies in the length of the line of sight in equation 2.2. As the distance to more and more pulsars become known, the Galactic Magnetic Field models will have the opportunity to become more and more anchored by constraints from them.

2.2 Synchrotron Emission

When relativistic cosmic ray electrons are accelerated radially by a magnetic field, the resulting radiation is called synchrotron emission. This is the kind of radiation that dominates full sky maps from radio to microwave frequencies. In the case of the Galactic Magnetic Field, this phenomenon

lets us probe the strength of the field perpendicular to our line of sight, as the intensity of the synchrotron emission is described as

$$I(\nu) \propto \int_{LOS} n_{cre}(\nu, l) B_{\perp}^{2} \nu^{-1} \mathrm{d}l. \tag{2.3}$$

Here, n_{cre} is the density of the relativistic cosmic ray electrons, dependent on the frequency of the radiation $\nu = 30$ GHz and the path length l (Fletcher et al., 2018). Contrary to rotation measures, which is calculated by observing how one ray of light is influenced by the Galactic Magnetic Field on its way through the galaxy, I is calculated by adding together the radiation caused by the Galactic Magnetic Field at each point along the LOS. Now, this is only the total intensity of the synchrotron emission. Another interesting part of this radiation is the polarized intensity I_p that depends on the Stokes parameters Q and U,

$$I_p \equiv \sqrt{Q^2 + U^2}. \tag{2.4}$$

These are defined as $Q = I\Pi \cos 2\psi \cos 2\chi$ and $U = I\Pi \sin 2\psi \cos 2\chi$, where the polarization degree $0 \leq \Pi \leq 1$ represents how much of the radiation is polarized and ψ and χ are two angles describing the polarization as shown in figure 2.3. ψ describes the orientation of the polarization, while χ denotes how linear the polarization is. It is clear from equation 2.4 that $\chi = \pi/2$ means no polarization, while $\chi = 0$ represents it being completely linear. In this case equation 2.4 simply becomes $PI \equiv I\Pi$. The factor of two in front of ψ is there because any polarization ellipse is indistinguishable from itself when rotated by 180 degrees, while it being in front of χ indicates that any ellipse is identical if it is rotated by 90 degrees and its semi-axis lengths are swapped. Interestingly, if the final Stokes parameter $V = I\Pi \sin 2\chi$ (otherwise not relevant to this paper) is added then $I\Pi$, 2χ and 2ψ are the spherical coordinates corresponding to the cartesian coordinates Q, U and V.

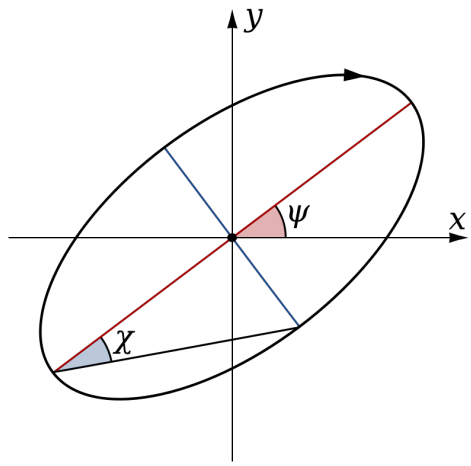

Figure 2.3: A visual representation of a polarization ellipse and how ψ and χ influence its shape.

As synchrotron emission intrinsically is very linearly polarized, it theoretically has a polarization degree Π around 75 %. The observed polarization fraction $p = I_p/I$ would be interesting to compare to Π, but is unfortunately still unavailable due to other kinds of radiation at the frequency which synchrotron emission is being observed at, in addition to depolarizing effects between the source and the observer. This is one of the biggest downsides of probing at radio frequencies, as these effects create a kind of "polarization horizon" behind which almost no polarization can be observed. One such effect could be the aforementioned Faraday rotation, which also introduces another issue: If the synchrotron emission we observe is Faraday rotated, then Q and U and by extension I_p will be dependent on RM, and different observables not being independent of each other is something to avoid.

There are also other sources of synchrotron emission in the galaxy than just the Galactic Magnetic Field polluting the data set, for instance possible

supernova remnants like the Northern Spur. These are especially prevalent in the disc, and to counteract them a polarization mask can be imposed on the data set to remove regions of the sky with suspiciously high I_p values that are likely to originate from local structures. An example of such a mask can also be found in section 3 of Jansson and Farrar (2012).

Another thing that complicates the accuracy of equation 2.3 is the uncertainty of n_{cre}, a parameter that obviously has a big impact on I and then also I_p. It is normal practice to assume equipartition of energy between cosmic rays and the Galactic Magnetic Field and that cosmic ray electrons contain 1 % of the total cosmic ray energy or number density (Beck and Krause, 2005), which makes it so that n_{cre} and $|B|^2$ are perfectly correlated at all scales. There are few direct verifications of this assumption, though, and the ones that exist are inconclusive. The two parameters have actually been found to be statistically independent at scales of 100 pc through test particle simulations of cosmic ray propagation in random magnetic fields (Seta et al., 2018), which might mean that while the assumption of equipartition of energy between Cosmic Rays and the Galactic Magnetic Field is effective at scales of kpc, it does not hold at the scales of the turbulent Galactic Magnetic Field.

2.3 Small-Scale Random Fields

One of the most challenging parts of the Galactic Magnetic Field to model is the random fields that originate from turbulence in the interstellar medium due to the massive amount of interconnected components constantly interacting and delivering feedback to each other. For a long time it was normal procedure to assume these fields were Gaussian and followed a power law with a certain coherence length between 10 pc and 100 pc. However, the sources of these fields are in fact not Gaussian. Instead, motivated by the observables discussed above, a phenomenological attempt at improving the modeling of the small-scale magnetic fields splits it into two components:

Ordered random fields and isotropic random fields (Fletcher et al., 2018, Jaffe, 2019).

The ordered random field might originate from Galactic shear or a shock wave compressing an isotropic field, and is defined by its contribution to rotation measures averaging to zero. It does this by following the direction of the coherent large-scale regular field while the orientation of the field is random, such that the contributions to the orientation-sensitive rotation measures cancel each other out. Due to $B_{\perp}^2$ of the ordered random field and the coherent field being indistinguishable from each other, I and I_p look the exact same for the two, and it is therefore very difficult to actually identify this kind of field, because the rotation measures being zero might as well mean that the direction of the field is perpendicular to the line of sight of the observer. The one-dimensionality of the randomness in the ordered random field somewhat resembles a first-order approximation of the turbulence in the interstellar medium, which makes it very interesting in terms of studying the origin of the turbulence.

On the other hand, the isotropic random field is generated by turbulence in ionized gas, is completely random in both its direction and orientation, and thus only contributes to I. The rotation measures average to zero for similar reasons as for the ordered random fields, while I_p does the same because the isotropic nature of the field removes the high polarisation degree of the synchrotron emission which comes from all of the radiation being produced in the same manner by similar sources. Due to this, the isotropic random field is much easier to identify than the ordered random field, but as was noted in section 2.2, the value of I_p is often lowered – sometimes all the way to zero – through depolarizing effects between the source and the observer. It is also possible to find traces of this type of field by looking at the variance in rotation measures and I_p (Haverkorn et al., 2004), because while they average to zero, an isotropic component in the Galactic Magnetic Field would increase the variance of the observables both along the LOS and across the sky.

2.4 Electron Densities

Another important thing about the simulation of rotation measure and synchrotron emission is, as is apparent from equations 2.2 and 2.3, the densities of thermal free electrons and relativistic electrons respectively. When the rotation measures and synchrotron emissions will be simulated from Galactic Magnetic Field models later in the thesis, the models that will be used for the electron densities are both mentioned by Jansson and Farrar (2012). For the relativistic electrons, the density will take the form

$$n_{cre}(r, z) = n_{cre,0} e^{-r/h_r} \operatorname{sech}^2(z/h_z) \tag{2.5}$$

as the model adopted by WMAP (Page et al., 2007). The normalization factor $n_{cre,0}$ is decided such that $n_{cre}(Earth) = 4.0 \times 10^{-5}/\text{cm}^3$, the observed value at Earth. r is the distance from the Galactic centre projected onto the Galactic plane and z is the vertical position above said plane. The remaining parameters are set to $h_r = 5$ kpc and $h_z = 1$ kpc as these are the original WMAP parameters.

For the thermal free electrons, the model that will be used is NE2001, developed by Cordes and Lazio (2002). This model splits the density n_e into a sum of several components representing different parts of the interstellar medium. The first part is the smooth component, which is made up of contributions from four different parts. There is a thick disk of scale height 1 kpc and scale radius of 20 kpc and a thin disk with scale radius on the short side of 9 kpc and a big drop in contribution when approaching 0.5 kpc both above and under the Galactic plane. In addition there are components from the Galactic centre and the spiral arms. The Galactic centre component has a scale height of 26 pc and a scale radius of 145 pc, so it covers only a very small area. In terms of the spiral arms, each arm has its own electron density. Of note is that the spiral arms are modelled as overdense regions, even though this is not the case astrophysically due to the enhanced star formation that takes place in the spiral arms causing under-

densities as well as overdensities. This completes the smooth component of the model.

Next there is a component that represents the interstellar medium local to Earth. This component itself is also composed of four components coming from four regions close to the Sun, with each having their own density contribution: Centered around the Sun there is a local hot bubble, there is a component from the well known North Polar Spur, in the third quadrant there is a local superbubble, and the last region is a low density region in the first quadrant. Obviously not all of the regions contribute to every position in the local interstellar medium, which the calculation of its electron density reflects. While in the local interstellar medium, the contribution from the smooth component is completely ignored, such that at least one of the smooth component and the local interstellar region component is zero at all times.

The last two density components belong to regions of low density called voids and regions of intense scattering called clumps. If the model finds itself in an area defined as a void, only the densities from the void and clump components count towards the total electron density. All of the clump and void regions are identified by their position, and each have its own set electron density.

In summary, to calculate the thermal free electron density at a point in the galaxy, the NE2001 model first checks whether the point is in the local interstellar medium or a void. If it is, only the components belonging to that region make up the total density, with the addition of possible clump contributions in the case of a void. If the point is in neither, the electron density is found by adding the contributions from the thick and thin disks, the spiral arms and the Galactic centre together to form the smooth component. The functional forms of all these components can be found in Cordes and Lazio (2002).

Chapter 3

Galactic Field Models

In 1937, Hannes Alfvén argued that if the Galaxy contains plasma, it could carry electrical currents that would give rise to magnetic fields (Alfvén, 1937), and thus became the first to theorize that there could be magnetic fields throughout the Milky Way. Then, in 1949, Enrico Fermi proposed that a Galactic Magnetic Field is responsible for the acceleration of cosmic rays (Fermi, 1949). Over the next decades an observational basis for this theory was slowly built up as it became apparent to researchers that synchrotron radiation from cosmic ray electrons was the origin of the observed Galactic radio emission. Of special note was the detection of linearly polarized radio waves from the Crab nebula by Mayer et al. (1957) that strongly suggested the presence of the aforementioned synchrotron process, and Cooper and Price (1962) confirming the effects of Faraday rotation on radiation from the radio source Centaurus A.

Over the last two decades, researchers have started to build increasingly complex numerical models for the Galactic Magnetic Field and used them to produce simulated observables to compare with observed quantities in an attempt to more completely understand the shape and strenght of the field. In this chapter two such models will be presented.

3.1 Jansson-Farrar model

Field	Best fit parameters	Description
Disk	$b_1 = 0.1 \pm 1.8$ μG	
	$b_2 = 3.0 \pm 0.6$ μG	
	$b_3 = -0.9 \pm 0.8$ μG	
	$b_4 = -0.8 \pm 0.3$ μG	field strengths at $r = 5$ kpc
	$b_5 = -2.0 \pm 0.1$ μG	
	$b_6 = -4.2 \pm 0.5$ μG	
	$b_7 = 0.0 \pm 1.8$ μG	
	$b_8 = 2.7 \pm 1.8$ μG	inferred from $b_1, ..., b_7$
	$b_{ring} = 0.1 \pm 0.1$ μG	ring at 3kpc $< r <$ 5 kpc
	$h_{disk} = 0.40 \pm 0.03$ kpc	height of disk/halo transition
	$w_{disk} = 0.27 \pm 0.08$ kpc	transition width
Toroidal halo	$B_n = 1.4 \pm 0.1$ μG	northern halo scale field strength
	$B_s = -1.1 \pm 0.1$ μG	southern halo scale field strength
	$r_n = 9.22 \pm 0.08$ kpc	transition radius, north
	$r_s > 16.7$ kpc	transition radius, south
	$w_h = 0.20 \pm 0.12$ kpc	width of cutoff in radial direction
	$z_0 = 5.3 \pm 1.6$ kpc	vertical scale height
X-field	$B_X = 4.6 \pm 0.3$ μG	field strength at origin
	$\Theta_X^0 = 49 \pm 1^\circ$	elev. angle at $z = 0$, $r > r_X^c$
	$r_X^c = 4.8 \pm 0.2$ kpc	radius where $\Theta_X^c = \Theta_X$
	$r_X = 2.9 \pm 0.1$ kpc	exponential scale length
striation	$\gamma = 2.92 \pm 0.14$	striation rescaling

Table 3.1: Parameters for the Jansson-Farrar model with $1 - \sigma$ intervals, as found in Jansson and Farrar (2012).

The Jansson-Farrar model (Jansson and Farrar, 2012) is one of the most recent and accurate models. This model disentangles the large-scale regular field and the so-called striated random fields by way of their different contributions to the Faraday rotation measures and the intensity and polar-

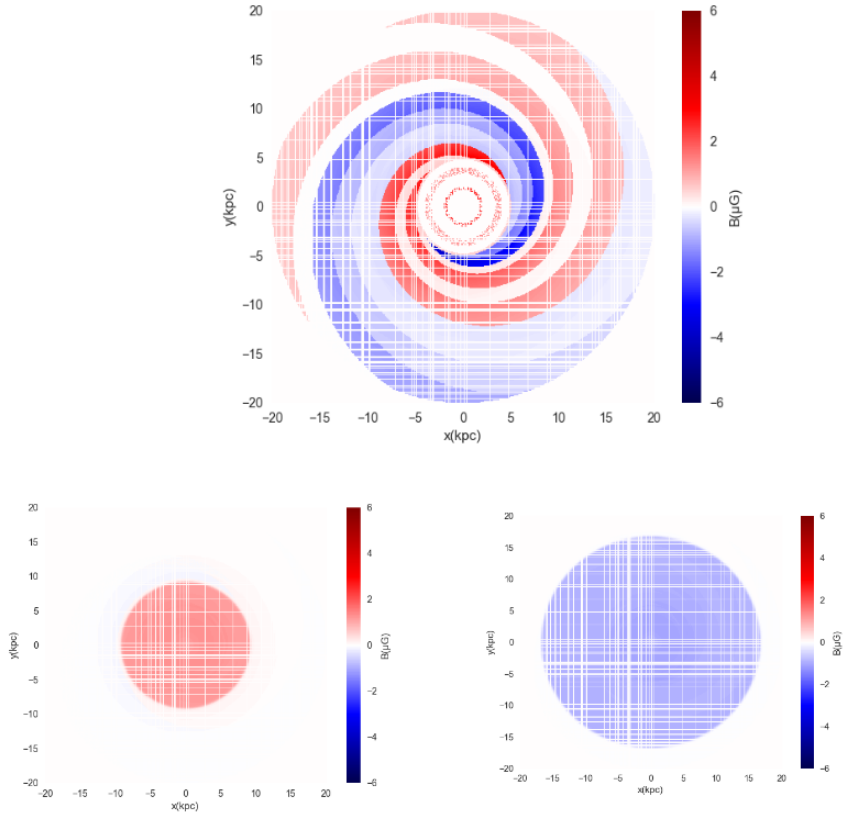

Figure 3.1: The Galactic Magnetic Field in the x-y-plane at, clockwise from the top, $z = 0$ kpc, $z = -1$ kpc and $z = 1$ kpc as described by the Jansson-Farrar model. Positive azimuthal direction gives positive values for the field strength.

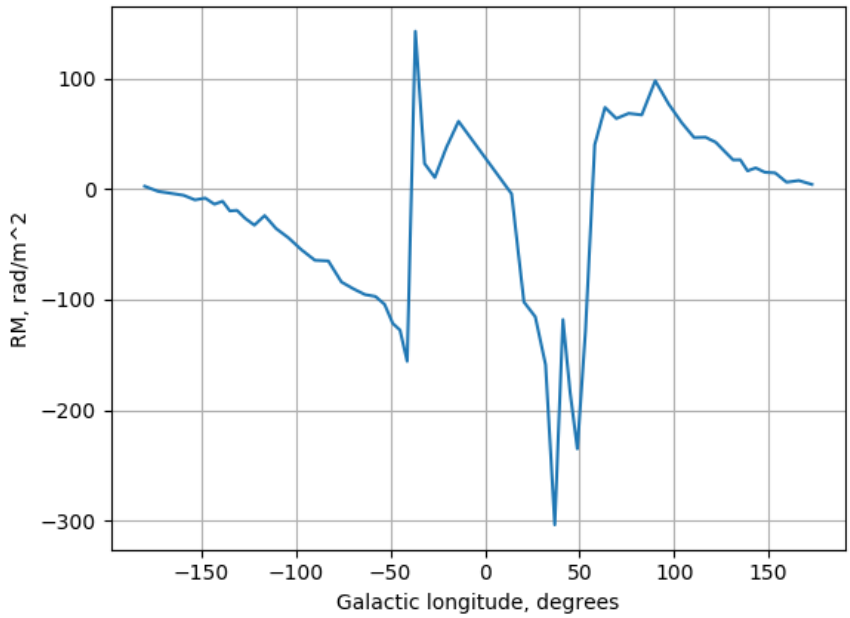

Figure 3.2: Rotation measures for the Jansson-Farrar model between -180 and 180 degrees Galactic longitude in the Galactic plane. The direction of the Galactic center is at 0 degrees. The model for n_e is as described in section 2.4.

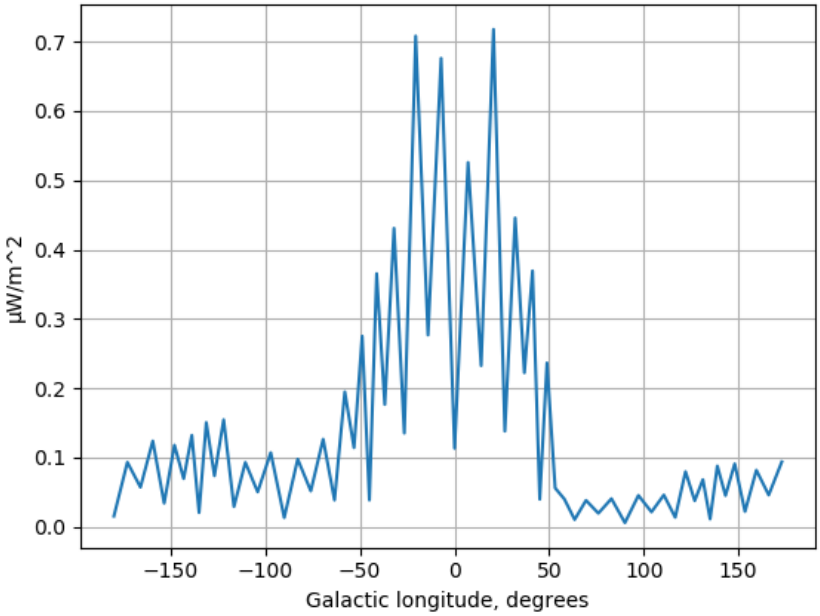

Figure 3.3: Synchrotron emission for the Jansson-Farrar model between -180 and 180 degrees Galactic longitude in the Galactic plane. The direction of the Galactic center is at 0 degrees. The model for n_{cre} is described in section 2.4.

ized intensity of synchrotron emission. While the regular field contributes to all three, the striated random field – being an ordered random field as was discussed in 2.3 – does not contribute to rotation measures because of its changing sign.

For the following description we use cartesian coordinates (x, y, z) and cylindrical coordinates (r, ϕ, z), with the Galactic centre at the origin and the Earth at $(x, y, z) = (0, 8.5, 0)$ kpc. For $r > 20$ kpc and a sphere of radius 1 kpc around the Galactic centre the field is set to zero.

3.1.1 Large-scale regular field

The large-scale regular field is in this model built up of three separate components: the disk field, the toroidal halo field and the out-of-plane field. All of these are divergenceless, and are subject to flux conservation even though that is a very constrictive, though important, constraint. All parameters mentioned can be found in table 3.1.

The disk component of the field is defined for all $r \in [3, 20]$ kpc, and is purely azimuthal with strength b_{ring} for $r \in [3, 5]$ kpc, in the 'molecular ring'. For $r > 5$ kpc, the field follows eight logarithmic spiral regions with a pitch angle $i = 11, 5°$. This value describes the angle with which the spiral arms protrude from the circumference of the molecular ring. The field strength b_j in spiral region j is defined at $r = 5$ kpc and goes as r^{-1}. The lines separating these spiral regions are given by

$$r = r_{-x} \exp(\phi \tan(90° - i)), \tag{3.1}$$

where $r_{-x} = 5.1, 6.3, 7.1, 8.3, 9.8, 11.4, 12.7, 15.5$ kpc represents the radii where the spirals cross the positive y-axis, and the direction of the magnetic field is given by $\hat{b} = \sin(i)\hat{r} + \cos(i)\hat{\phi}$. The disk field is symmetrical with respect to the plane at $z = 0$, and it extends over a total height of h_{disk}. At the extremities of this interval the disk field transitions to the

toroidal halo field as described by the transitional function

$$L(z, h, w) = (1 + e^{-2(|z|-h)/w}), \tag{3.2}$$

where w_{disk} decides the width of the transition region. One can multiply the disk component of the field with $(1 - L(z, h_{disk}, w_{disk}))$ while the toroidal halo component is multiplied by $L(z, h_{disk}, w_{disk})$ to get the true strength of the field components.

The toroidal halo field is, as its name suggests, purely azimuthal, and is defined as

$$B_\phi^{tor} = \begin{cases} e^{-|z|/z_0} L(z, h_{disk}, w_{disk}) B_n (1 - L(r, r_n, w_h)) & \text{for } z > 0, \\ e^{-|z|/z_0} L(z, h_{disk}, w_{disk}) B_s (1 - L(r, r_s, w_h)) & \text{for } z < 0 \end{cases} \tag{3.3}$$

with the transitional function mentioned above included. Here, B_n and B_s represent the amplitude of the field strength in the northern and southern parts of the galaxy respectively. Similarly, r_n and r_s represent the extent of the halo field in the radial direction in those regions. w_h controls the width of the region where the halo field cuts off, and z_0 sets the scale height.

Finally, we have the out-of-plane component. As we have seen, both the large-scale component and halo component are confined to planes parallel to the $x-y$-plane, and so this third component of the regular field will represent the parts that are not. It is often called the "X-field" for short, due to its appearance when viewed from the plane of the galactic disk as seen in figure 3.4. The field is described in terms of r_p, which is the radius at which the field line passing through any point (r, z) crosses the z-axis. Θ_X is the elevation angle of the field lines, and $\Theta_X = 90°$ when $r = 0$ kpc. From there it decreases linearly with r until r becomes greater than the galactocentric radius r_X^c, where it becomes the constant Θ_X^0. The field strength in the mid-plane is defined as

$$b_X(r_p) = B_X e^{-r_p/r_X}, \tag{3.4}$$

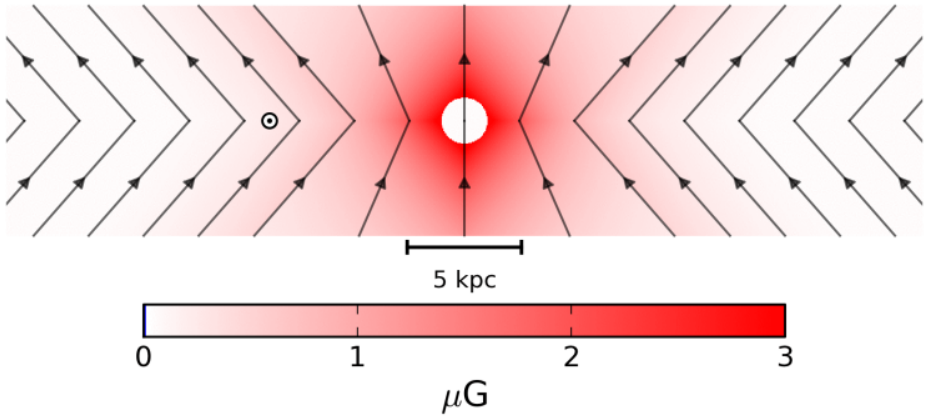

Figure 3.4: The X-field as seen in a $x - z$ slice of the galaxy. The arrows show the direction of the field and the dot marks the position of the sun. From Jansson and Farrar (2012).

where B_X is the overall amplitude of the X-field. Now, the requirement $\nabla \cdot \boldsymbol{B} = 0$ is enough to characterize the field. For $r > r_X^c$ we then get that the field strength is $b_X(r_p)r_p/r$, with

$$r_p = r - |z|/\tan(\Theta_X^0). \tag{3.5}$$

In the region where $r < r_X^c$ and Θ_X varies, the field strength becomes $b_X(r_p)(r_p/r)^2$ and we get r_p and Θ_X like this:

$$r_p = \frac{r r_X^c}{r_X^c + |z|/\tan(\Theta_X^0)} \tag{3.6}$$

$$\Theta_X(r, z) = \tan^{-1}\left(\frac{|z|}{r - r_p}\right). \tag{3.7}$$

3.1.2 Striated random fields

The so-called striated random fields are the same as the ordered random fields mentioned in section 2.3, and are thus fields that are always aligned along a particular axis – predominantly the direction of the regular field – on a larger scale. Meanwhile, its strength and sign may vary on the small scale, giving the impression of a striated pattern from which it gets its name. By adding a multiplicative factor to the calculation of the synchrotron intensity, the possibility of the striated random fields is included in the model while also having an easy way of removing them by setting the factor to zero. These fields are parametrized as $B^2_{stri} = \beta B^2_{reg}$ with $\beta \geq 0$, and let the factor be a free parameter in the large-scale model. As is apparent, the striated fields are always aligned with the regular field, but is not necessarily of the same strength. Using only one independent factor for this parametrization also means that the striated fields have the same relative strength throughout the entire galaxy.

3.2 The Sun *et al.* model

In their paper about radio observational constraints on Galactic 3D-emission models (Sun et al., 2008), Sun *et al.* look at three different models for the Galactic Magnetic Field, two with axi-symmetric spirals where one has field reversals in rings (ASS+RING) and the other has field reversals along its spiral arms (ASS+ARM), and one model with bi-symmetric spirals (BSS). Here we will focus on the ASS+RING model, as it was found to be the best fit to the data they were working with, including rotation measures.

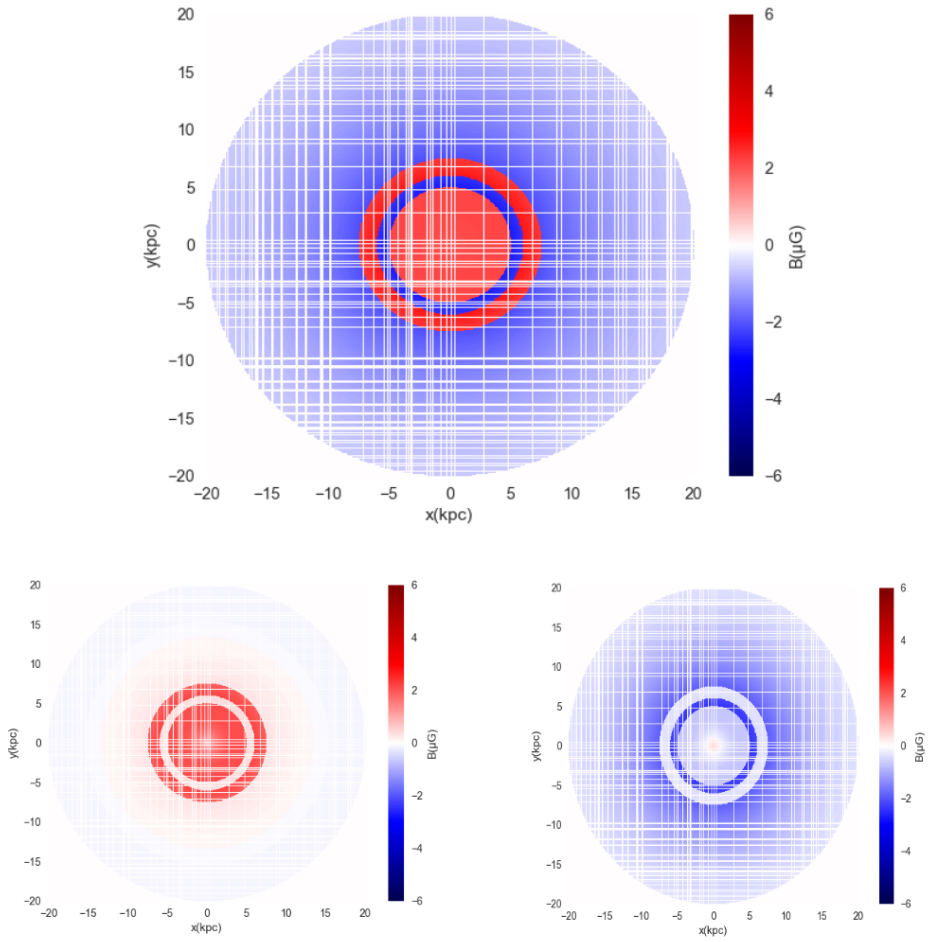

Figure 3.5: The same as figure 3.1, but for the Sun *et al.* model. The position of the Earth is at $(x, y) = (0, 8.5)$ kpc.

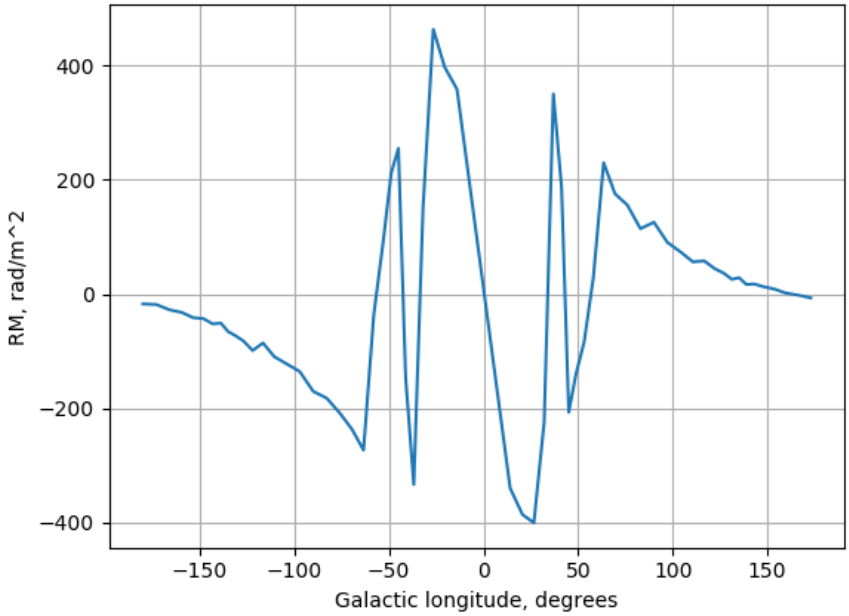

Figure 3.6: The same as figure 3.2, but for the Sun *et al.* model.

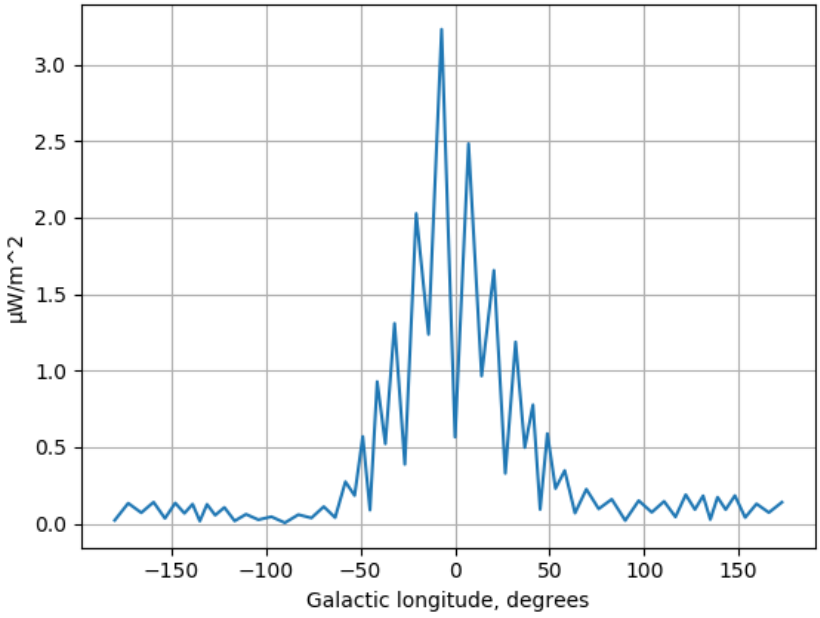

Figure 3.7: The same as figure 3.3, but for the Sun *et al.* model.

Field	Parameters	Description
Disk	$R_0 = 10$ kpc	scale radius
	$R_c = 5$ kpc	radius from which the spirals protrude
	$R_\odot = 8.5$ kpc	adjusts B_0
	$z_0 = 1$ kpc	vertical scale height
	$B_0 = 2\ \mu$G	scale strength of field for $r \geq R_c$
	$B_c = 2\ \mu$G	scale field strength for $r < R_c$
Halo	$B_0^H = 10\ \mu$G	scale field strength
	$z_0^H = 1.5$ kpc	height of max field strength
	$z_1^H = 0.2$ kpc for $\lvert z\rvert < z_0^H$	Scales difference between z and z_0^H
	$z_1^H = 0.4$ kpc otherwise	
	$R_0^H = 4$ kpc	radius of max field strength

Table 3.2: Parameters for the Sun *et al.* model.

3.2.1 Regular field

The regular field of the ASS+RING model has only two components; a disk field and a halo field. The general form of the disk field is written in cylindrical coordinates as

$$\begin{aligned} B_r^D &= D_1(r,\phi,z)D_2(r,\phi,z)\sin i \\ B_\phi^D &= -D_1(r,\phi,z)D_2(r,\phi,z)\cos i \\ B_z^D &= 0. \end{aligned} \tag{3.8}$$

Here again $i = -12^\circ$ is the constant pitch angle of the spiral arms. The field in the directions of r and ϕ are products of two functions $D_1(r,\phi,z)$ and $D_2(r,\phi,z)$, where the first constrains the spatial variation of the field strength and the latter introduces asymmetries and reversals. All the parameters can be found in table 3.2. D_1 is always defined as

$$D_1(r,z) = \begin{cases} B_0 \exp\left(-\frac{r-R_\odot}{R_0} - \frac{|z|}{z_0}\right) & \text{for } r > R_c \\ B_c \exp\left(-\frac{|z|}{z_0}\right) & \text{for } r \leq R_c. \end{cases} \tag{3.9}$$

As for D_2, we write

$$D_2(r) = \begin{cases} +1 & r > 7.5 \text{ kpc} \\ -1 & 6 \text{ kpc} < r \leq 7.5 \text{ kpc} \\ +1 & 5 \text{ kpc} < r \leq 6 \text{ kpc} \\ -1 & r \leq 5 \text{ kpc}, \end{cases} \tag{3.10}$$

where +1 means clockwise direction seen from the Galactic North Pole. Note that the minus sign in the azimuthal part of equation 3.8 makes it so that the intervals with $D_2 < 0$ gives positive azimuthal direction as clockwise and positive azimuthal direction are opposite to each other. This way of defining the field reversals, with them being in specific radial intervals, is what gave this model the name ASS+RING.

As for the halo field, Sun *et al.* chose a torus field that is antisymmetric with respect to the Galactic plane at $z = 0$ due to an asymmetry in the RM maps between those regions. We write the strength of the field as

$$B^H_{strength}(r,z) = B^H_0 \frac{1}{1 + \left(\frac{|z|-z^H_0}{z^H_1}\right)^2} \frac{r}{R^H_0} \exp\left(-\frac{r - R^H_0}{R^H_0}\right) \tag{3.11}$$

and then have

$$B^H_\phi = \begin{cases} B^H_{strength} & z \geq 0 \\ -B^H_{strength} & z < 0. \end{cases} \tag{3.12}$$

Whereas the Jansson-Farrar model uses a transitional function to modulate the transitional area between the disk field and the halo field, the Sun

et al. model is content to simply add the disk and halo field together to form the complete regular field.

3.2.2 Random field

In their paper, Sun *et al.* discuss several ways to produce more accurate models for the random fields, but decide not to use any of them in their final model (see Sun et al. (2008) for details). Instead, it is simply assumed that the strength of the random field follows a Gaussian distribution (as was briefly touched on in section 2.3) with an average of zero and a constant scatter in all directions, which gives the best value for the mean strength of the random field to be $B = 3\ \mu$G.

Chapter 4

Comparison and discussion

In this chapter the two Galactic Magnetic Field models presented in the previous chapter will be compared and discussed in terms of their shape, functional form and the rotation measure and synchrotron emission plots they produced. In addition, what modelling the Galactic Magnetic Field may look like in the future will be touched upon.

4.1 Models

Almost immediately upon inspecting figure 3.1 and 3.5 it is apparent that the Jansson-Farrar model is more complex in its structure by taking care to shape the spiral arms of the Galaxy. Meanwhile, the Sun *et al.* model is content with only considering the distance from the Galactic centre and the height above the Galactic plane, and letting the electron density models impose the structure of the Galaxy on the model as rotation measure and synchrotron emission are simulated. However, this does put pressure on these density models, and while the NE2001 model (Cordes and Lazio, 2002) for the thermal electron density is satisfactory in this regard, the model for the

relativistic electron density presented in equation 2.5 does leave something to be desired in terms of modelling the shape of the Galaxy.

It is also interesting to note the difference in field reversals between the two models. In the Sun *et al.* model the reversals are simply a case of radial distance from the Galactic centre, while in the Jansson-Farrar model they follow the spiral arms of the model. The reason for this is that the disk field of the Jansson-Farrar model is based on an article by Brown et al. (2007), who argue that the rotation measure data requires a magnetic reversal between the Sagittarius-Carina and Scutum-Crux arms in the fourth Galactic quadrant and thus decide to let the reversals follow the spiral arms. While Sun *et al.* do discuss a model with a reversal inspired by Brown *et al.* called the ASS+ARM model (Sun et al., 2008) as was mentioned in section 3.2, they found that the model discussed in this thesis gave a better fit to the rotation measure data they used for comparison. It is worth noting that the only difference between their ASS+ARM model and the ASS+RING model is the functional form of D_2 in equation 3.8, so its resemblance to the Jansson-Farrar model ends at the inspiration for the field reversals.

Other than the spiral region structure and the different field reversals, the two models actually do similar things. They are both radially independent until $r = 5$ kpc, and outside that the field strength decreases following a strictly decreasing function, the Jansson-Farrar model as r^{-1} and the Sun *et al.* as e^{-r}.

Looking at the fields at $z = \pm 1$ kpc, it might look like the halo fields utilized by both Jansson and Farrar and Sun *et al.* agree on more than they disagree on, with the regular fields imposing the differences. In figure 3.5 the reversal rings of the Sun *et al.* model are very visible, and in figure 3.1 one can see a hint of the spiral structure of the Jansson-Farrar model. When inspected more closely, though, relevant differences can be found. The main one is that the halo field of the Sun *et al.* model is zero at the Galactic centre due to the factor r/R_0^H in equation 3.11. Otherwise the radial parts of equations 3.11 and 3.3 are very similar. The vertical

parts are not as similar due to their functional forms being completely different, with the exponential function in equation 3.3 of the Jansson-Farrar model decreasing faster than the rational form in 3.11 of the Sun *et al.* model. Though the behaviour in the $z \to \infty$ limit is the same, there is a non-negligible difference for the relevant values of z which becomes very apparent when using the parameters from tables 3.1 and 3.2.

In the end, the Jansson-Farrar model is a newer and more accurate model than the Sun *et al.* model. It achieved $\chi^2/\text{dof} = 1.1$ compared to $\chi^2/\text{dof} = 1.3$ (Jansson and Farrar, 2012) by the Sun *et al.* model, where "dof" stands for degrees of freedom. Still, it is important to remember what was discussed in section 2.1 and 2.2 about the insecurities around the observations these models are trying to replicate and not just blindly accept them.

4.2 Observables

4.2.1 Synchrotron Intensity

Moving on to the simulated observables, first we look at the synchrotron intensities from figure 4.1 and the relative difference between the intensities produced by the two models in figure 4.2. The most obvious difference between the two is the region between -50 and 50 degrees Galactic longitude, with the Jansson-Farrar model yielding a much lower intensity than the Sun *et al.* model. As the only difference in the simulation of the two intensities is the strength of the field, it would seem that Sun *et al.* predicted stronger fields around the Galactic centre than Jansson and Farrar did. Looking at figure 3.1 and 3.5, this assumption makes sense as one can clearly see that the field strength in the centre of the Galaxy is much higher in the Sun *et al.* model.

Taking a look at the region with less than -50 degrees Galactic longitude, the synchrotron intensities produced by the two models are very much

alike, but comparing with the region that has a longitude of more than 50 degrees the same is not the case. The reason for this asymmetry is found in the figures describing the magnetic field models, figure 3.1 and 3.5. When the longitude is less than -50 degrees, the line of sight is passing through the outer parts of the first quadrant of the figure, and when more than 50 degrees the line of sight moves through this part of the second quadrant. In the Sun *et al.* model the fields in these two quadrants are the same due to the model being independent of the azimuthal angle ϕ, but that is not the case for the Jansson-Farrar model. There is a blue spiral arm moving through both quadrants right outside Earths position at $(x, y) = (0, 8.5)$ that is noticably stronger in the first quadrant than the second, making one of the main contributions to the intensity stronger there. In addition the line of sight passes one additional spiral arm in the first qaudrant compared to the second. Together, these phenomena provide reasons for the asymmetry in the synchrotron intensity produced by the Jansson-Farrar model.

4.2.2 Rotation Measures

Turning the attention to figure 4.3 and 4.4 and considering the broad strokes of the simulated rotation measures, the two models in question produce fairly similar behaviour, but with different amplitudes. The difference in minima and maxima correlates with the difference in synchrotron intensity around the Galactic centre, as the stronger fields produced in that area by the Sun *et al.* model produces larger contributions to the rotation measures as well.

Interestingly, the size of the extremities of the rotation measures produced by the Jansson-Farrar model are significantly different from each other, with the size of the maximum being around double the size of the minimum. The two extremities are positioned at ± 37 degrees Galactic longitude. Given that the clean antisymmetry in the extremities that the rotation measures produced by the Sun *et al.* model have is something you would expect because of its independence of the azimuthal angle ϕ, the dif-

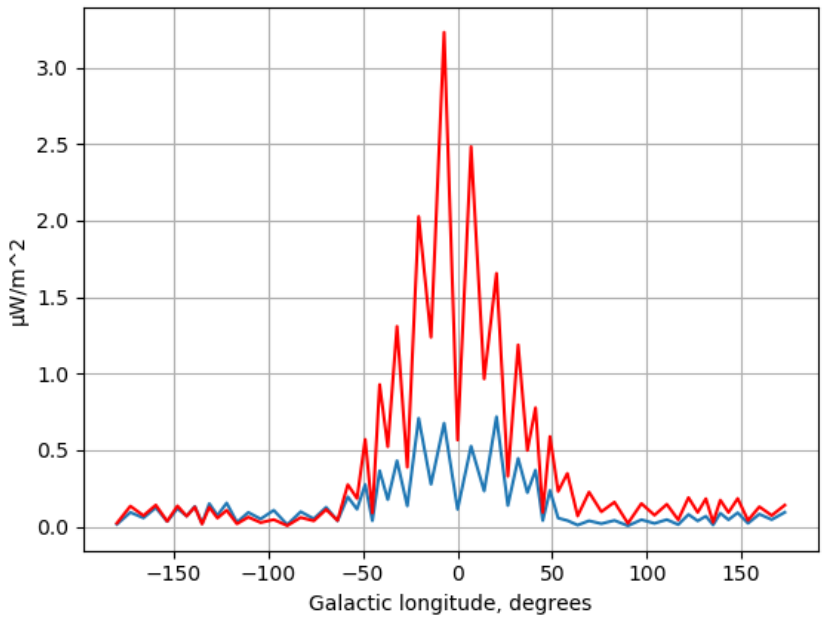

Figure 4.1: The synchrotron emission intensity I generated by the Jansson-Farrar model (blue) and the Sun *et al.* model (red) using the model for the relativistic cosmic ray electron density n_{cre} defined by equation 2.5. The points of Galactic longitude used are the same as for figure 3.3 and 3.7.

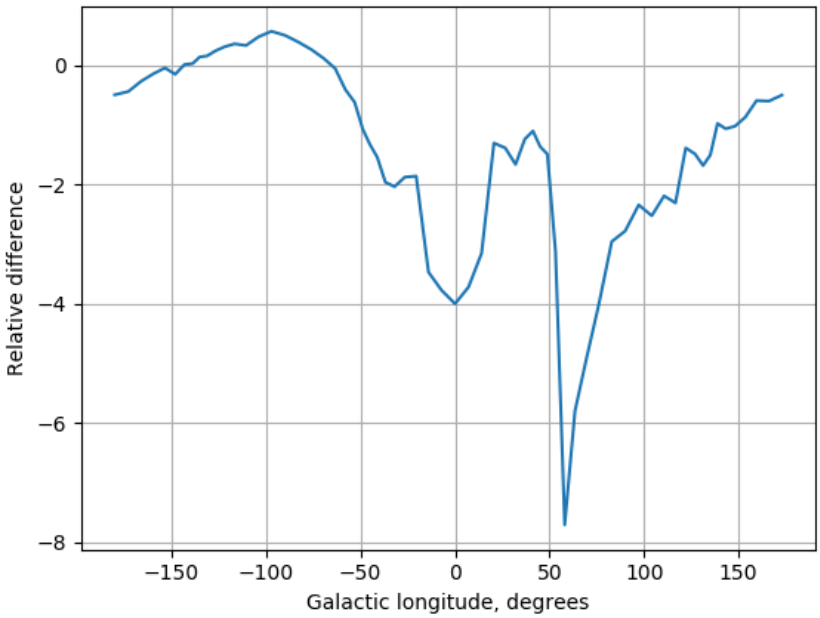

Figure 4.2: The relative difference in synchrotron intensity calculated by the Jansson-Farrar and Sun *et al.* models $((\mathrm{I}_{JF} - \mathrm{I}_{Sun})/\mathrm{I}_{JF})$ for the same points of Galactic longitude as figure 3.3 and 3.7.

ference in the size of the extremities in the rotation measures simulated by the Jansson-Farrar model is unlikely to be because of the thermal electron density model, because then it would be visible in the plot for the Sun *et al.* model too. It is therefore most likely something that comes from the magnetic field of the Jansson-Farrar model. The main differences will be found by examining the first and second quadrant of figure 3.1, as the line of sight passes through the first quadrant at -37 degrees and through the second at 37 degrees. In both, the main contributor to the rotation measure will be the red spiral arm just inside Earth's position at $(x, y) = (0, 8.5)$. Because it curls up to the molecular ring in the first quadrant while spiralling outwards in the second, the line of sight is inside the spiral arm for longer at 37 degrees than at -37 degrees, giving it more contributions to the rotation measure. Of course, there will be contributions from the field outside this spiral arm as well, but because the field in the spiral is both stronger and closer to being parallel to the line of sight than the field further out, it has a much larger impact on the rotation measures at the Galactic longitudes that coincide with the extremities produced by the Jansson-Farrar model.

Another very noticable difference between the two plots of figure 4.3 is the behaviour of the rotation measures simulated by the Sun *et al.* model around ± 37 degrees, where it produces a switch in sign that the Jansson-Farrar model does not. The most probable reason for this switch is the field reversal that exists in 6 kpc $< r \leq 7.5$ kpc, as the region containing this reversal is an area that the line of sight travels through at both -37 and 37 degrees Galactic longitude and represents field lines going the opposite way of the ones both inside and outside this region. Here the field lines will be very close to parallel to the line of sight as well, so the contributions to the rotation measures from this region will dominate compared to the weaker and less parallel field lines that the line of sight passes through further out. In addition there is no equivalent to this reversal in the Jansson-Farrar model, so it being a major difference between the two Galactic magnetic field models also supports it being the origin of this behaviour in the simulated rotation measures.

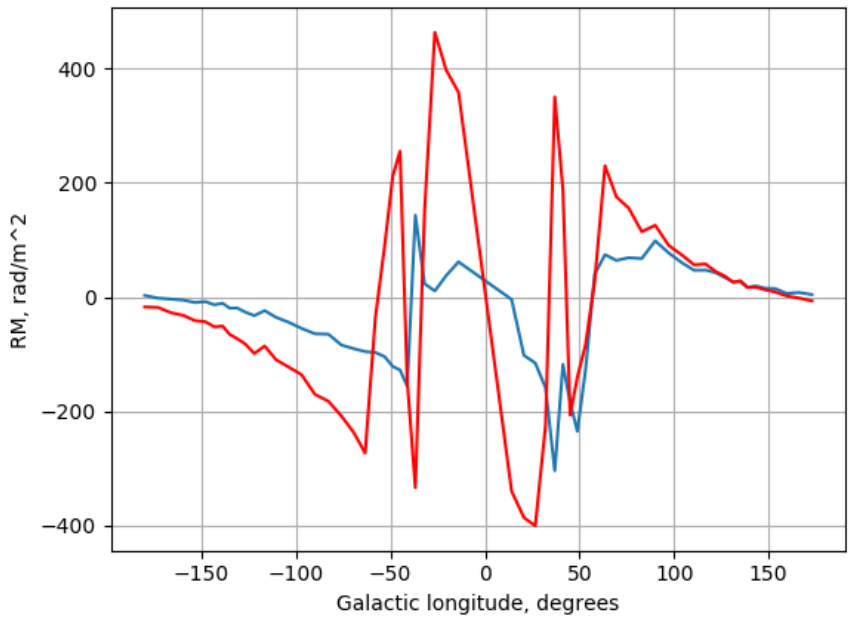

Figure 4.3: The Faraday rotation measure RM generated by the Jansson-Farrar model (blue) and the Sun *et al.* model (red) using the NE2001 model for the thermal electron density (Cordes and Lazio, 2002). The points of Galactic longitude used are the same as for figure 3.2 and 3.6.

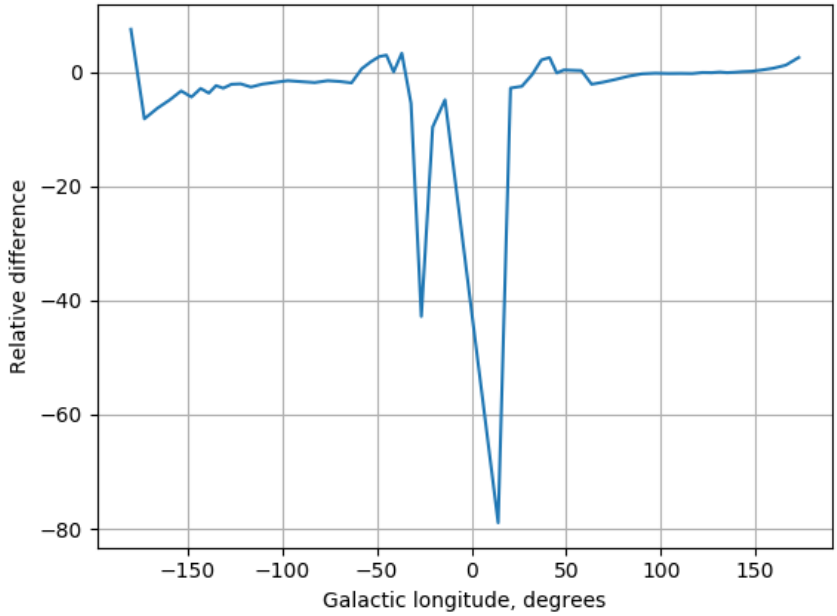

Figure 4.4: The relative difference in Rotation Measures calculated by the Jansson-Farrar and Sun *et al.* models $((\mathrm{RM}_{JF} - \mathrm{RM}_{Sun})/\mathrm{RM}_{JF})$ for the same points of Galactic longitude as figure 3.2 and 3.6.

4.2.3 Electron densities

Considering the role of the electron density models used to calculate the rotation measures and synchrotron intensities, figure 4.5 and 4.6 show that they both mainly control the amplitude of the integrals, suppressing them in regions of the Galaxy where there should be less interactable matter and thus less contributions. The behaviour, in terms of when they increase and decrease, of both the rotation measure and synchrotron emission plots are to a large extent intact.

4.3 Outlook

The way forward to better models for the Galactic magnetic field is twofold: To further build upon the models that are motivated by observation, and create models based on the physics of the Galaxy.

Both the Sun *et al.* and the Jansson-Farrar model are motivated by observations of the observables discussed in chapter 2, and the way forward with these kinds of models will be paved by more and better data. As the computer power available and the experience with building Galactic magnetic field models this way grows with time, so will also the potential complexity of the models. Looking at the most recent model discussed in this thesis, the Jansson-Farrar model, it is possible to make improvements on for instance the modelling of the spiral arms. In the current model, the magnetic field is the same for the entire breadth of the arm, which one would assume would not to be the case as there is more matter in the core of the arm than on the edges of it. This is of course something that also could be modelled by improved electron density models. As mentioned in section 2.1, finding the exact distance to more pulsars is also something that would greatly improve the data available to base new models on. Information about localized rotation measures can show more of how the field lines look in those regions as opposed to a single value representing all field

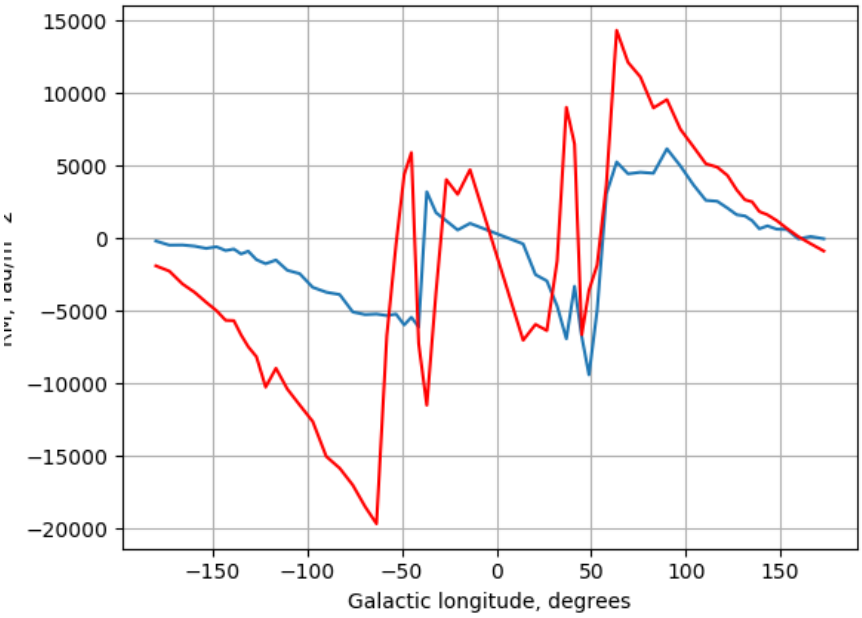

Figure 4.5: The Faraday rotation measure RM generated by the Jansson-Farrar model (blue) and the Sun *et al.* model (red) with the thermal electron density set to 1 for the entire Galaxy. The points of Galactic longitude used are the same as for figure 3.2 and 3.6.

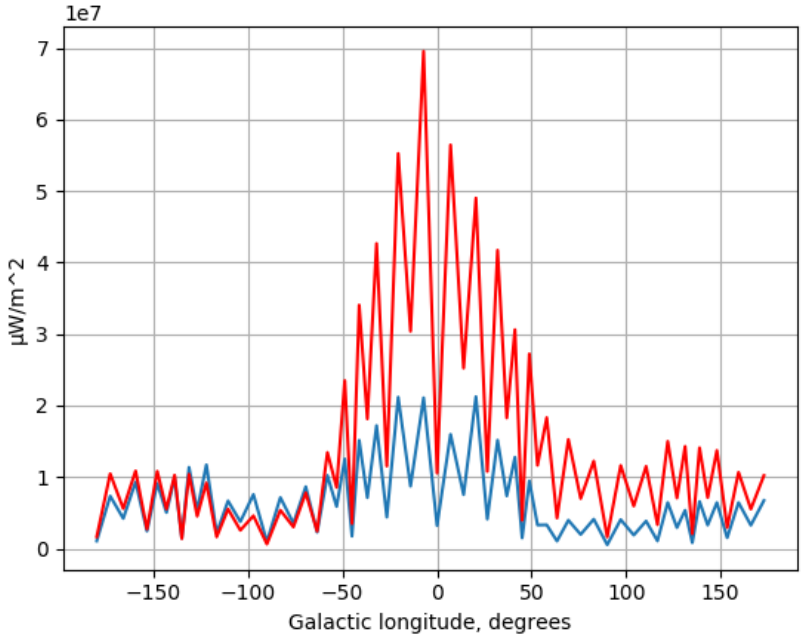

Figure 4.6: The synchrotron emission intensity I generated by the Jansson-Farrar model (blue) and the Sun *et al.* model (red) with the density of relativistic cosmic ray electrons set to 1 for the entire Galaxy. The points of Galactic longitude used are the same as for figure 3.3 and 3.7.

lines along a path of up to 28 kpc.

Some of the more exciting work being done in the field is the development of analytical models for the Galactic magnetic field based on what we know about the physics of the Milky Way. This was begun in 2013 by Terral and Ferrière (2014, 2017) and taken further in 2019 by Shukurov et al. (2019). While still a young field of study, making the models fairly simple as of yet, that will always be the starting point. These models – as well as the models based on observations – are all parametric, as non-parametric models do not yet exist. This is due to them being unfeasible to calculate because of the immense amount of values that has to be both calculated and handled, as such a model would require every point in 3D-space to hold a magnetic field vector. Despite that it is a goal of the IMAGINE Consortium to enable the building of non-parametric models of the Galactic magnetic field (Fletcher et al., 2018).

Of course, the true endgame will be to use both analytical and observationally motivated models together, to use what is known of the physics of the Galaxy to explain what is observed and to use knowledge of the physical dynamics of the Galaxy to consider what are good observations and what are not. That is the way forward if the Galactic magnetic field is ever to be truly understood.

Chapter 5

Conclusion

Comparing the Jansson-Farrar model and the Sun *et al.* model for the Galactic Magnetic field, the main differences are the form they take, how the magnetic field reversals are handled and how they model the small-scale random field. In terms of the form, the Jansson-Farrar model creates separate spiral arm regions with different field strengths, while the Sun *et al.* model is completely axisymmetric about the Galactic centre. The Jansson-Farrar model lets the field reversals follow the spiral arms as suggested by Brown *et al.* Brown et al. (2007), while the Sun *et al.* model simply place them at radial intervals. As for the small-scale random fields, the Jansson-Farrar model implements an ordered random field and Sun *et al.* simply uses the traditional Gaussian distribution. Otherwise both models have a constant field strength for $r < 5$ kpc and outside of that the field strength is strictly decreasing with r. Both have toroidal halo fields with similar behaviour. Looking at the simulated observables, the Sun *et al.* model consistently produces stronger contributions for both the Faraday rotation measures and synchrotron intensity, likely due to its more homogeneous field. The shape of these simulated plots, however, are quite similar except for a couple of differences probably due to the differing choices

for the magnetic field reversals and, again, the difference in homogeneity between the two models.

Bibliography

R. Adam, P. A. R. Ade, N. Aghanim, Y. Akrami, M. I. R. Alves, F. Argüeso, M. Arnaud, F. Arroja, M. Ashdown, and et al. Planck2015 results. *Astronomy & Astrophysics*, 594:A1, Sep 2016. ISSN 1432-0746. doi: 10.1051/0004-6361/201527101. URL http://dx.doi.org/10.1051/0004-6361/201527101.

H. Alfvén. Cosmic radiation as an intra-galactic phenomenon. *Ark. f. mat., astr. o. fys.*, 25B(29), 1937.

R. Beck and M. Krause. Revised equipartition & minimum energy formula for magnetic field strength estimates from radio synchrotron observations. *Astronomische Nachrichten*, 326:414–427, 2005.

R. Beck, A. Shukurov, D. Sokoloff, and R. Wielebinski. Systematic bias in interstellar magnetic field estimates. *Astronomy & Astrophysics*, 441 (2):99–107, November 2003.

M. A. Brentjens and A. G. de Bruyn. Faraday rotation measure synthesis. *Astronomy & Astrophysics*, 441(3):1217–1228, October 2005.

J. C. Brown, M. Haverkorn, B. M. Gaensler, A. R. Taylor, N. S. Bizunok, N. M. McClure-Griffiths, J. M. Dickey, and A. J. Green. Rotation measures of extragalactic sources behind the southern galactic plane: New insights into the large-scale magnetic field of the inner milky way. *The Astrophysical Journal*, 663(1):258–266, July 2007. ISSN 1538-4357. doi: 10.1086/518499. URL http://dx.doi.org/10.1086/518499.

B. J. Burn. On the depolarization of discrete radio sources by faraday dispersion. *Monthly Notices of the Royal Astronomical Society*, 133: 67–83, July 1966.

B. F. C. Cooper and R. M. Price. Faraday rotation effects associated with the radio source centaurus a. *Nature*, 196:1084—-1085, September 1962.

J. M. Cordes and T. J. W. Lazio. Ne2001.i. a new model for the galactic distribution of free electrons and its fluctuations, 2002.

E. Fermi. On the origin of the cosmic radiation. *Phys. Rev.*, 75:1169–1174, Apr 1949. doi: 10.1103/PhysRev.75.1169. URL https://link.aps.org/doi/10.1103/PhysRev.75.1169.

F. B. T. E. A. Fletcher, P. Girichidis, S. Hackstein, M. Haverkorn, J. R. Hörandel, T. Jaffe, J. Jasche, M. Kachelrieß, K. Kotera, C. Pfrommer, J. P. Rachen, L. F. S. Rodrigues, B. Ruiz-Granados, A. Seta, A. Shukurov, G. Sigl, T. Steininger, V. Vacca, E. van der Velden, A. van Vliet, and J. Wang. Imagine: a comprehensive view of the interstellar medium, galactic magnetic fields and cosmic rays. *Journal of Cosmology and Astroparticle Physics*, 2018, August 2018.

M. Haverkorn, B. M. Gaensler, N. M. McClure-Griffiths, J. M. Dickey, and A. J. Green. Magnetic fields and ionized gas in the inner galaxy: An outer scale for turbulence and the possible role of h ii regions. *The Astrophysical Journal*, 609:776–784, 2004.

T. Jaffe. Practical modeling of large-scale galactic magnetic fields: Status and prospects. *Galaxies*, 7(2):52, Apr 2019. ISSN 2075-4434. doi: 10.3390/galaxies7020052. URL http://dx.doi.org/10.3390/galaxies7020052.

R. Jansson and G. R. Farrar. A new model of the galactic magnetic field. *The Astrophysical Journal*, 757, 2012.

C. H. Mayer, T. P. McCullough, and R. M. Sloanaker. Evidence for Polarized Radio Radiation from the Crab Nebula. *The Astrophysical Journal*, 126:468, November 1957. doi: 10.1086/146419.

N. Oppermann, H. Junklewitz, G. Robbers, M. R. Bell, T. A. Enßlin, A. Bonafede, R. Braun, J. C. Brown, T. E. Clarke, I. J. Feain, and et al. An improved map of the galactic faraday sky. *Astronomy & Astrophysics*, 542:A93, Jun 2012. ISSN 1432-0746. doi: 10.1051/0004-6361/201118526. URL http://dx.doi.org/10.1051/0004-6361/201118526.

L. Page, G. Hinshaw, E. Komatsu, M. R. Nolta, D. N. Spergel, C. L. Bennett, C. Barnes, R. Bean, O. Dore, and J. D. et al. Three-year wilkinson microwave anisotropy probe(wmap) observations: Polarization analysis. *The Astrophysical Journal Supplement Series*, 170(2): 335–376, Jun 2007. ISSN 1538-4365. doi: 10.1086/513699. URL http://dx.doi.org/10.1086/513699.

A. Seta, A. Shukurov, T. S. W. P. J. Bushby, and A. P. Snodin. Relative distribution of cosmic rays and magnetic fields. *Monthly Notices of the Royal Astronomical Society*, 473(4):4544–4557, February 2018.

A. Shukurov, L. F. S. Rodrigues, P. J. Bushby, J. Hollins, and J. P. Rachen. A physical approach to modelling large-scale galactic magnetic fields. *Astronomy & Astrophysics*, 623:A113, Mar 2019. ISSN 1432-0746. doi: 10.1051/0004-6361/201834642. URL http://dx.doi.org/10.1051/0004-6361/201834642.

X. H. Sun, W. Reich, A. Waelkens, and T. Enßlin. Radio observational constraints on galactic 3d-emission models. *Astronomy & Astrophysics*, 477(2):573–592, January 2008.

P. Terral and K. Ferrière. Analytical models of x-shape magnetic fields in galactic halos. *Astronomy & Astrophysics*, 561:A100, Jan 2014. ISSN 1432-0746. doi: 10.1051/0004-6361/201322966. URL http://dx.doi.org/10.1051/0004-6361/201322966.

P. Terral and K. Ferrière. Constraints from faraday rotation on the magnetic field structure in the galactic halo. *Astronomy & Astrophysics*, 600:A29, Mar 2017. ISSN 1432-0746. doi: 10.1051/0004-6361/201629572. URL http://dx.doi.org/10.1051/0004-6361/201629572.

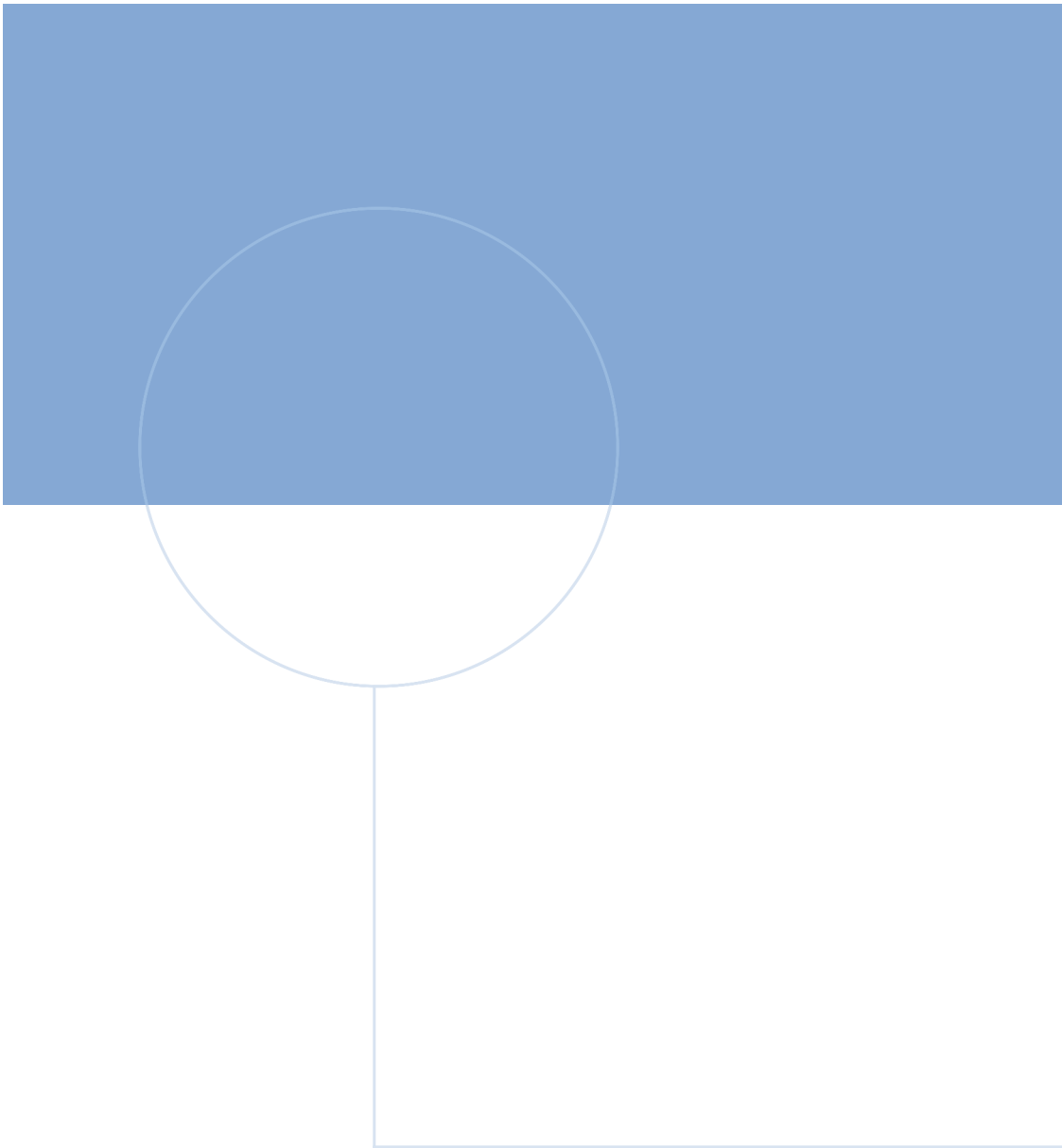

NTNU
Norwegian University of
Science and Technology